Transp Porous Med (2010) 83:333–347
DOI 10.1007/s11242-009-9444-8

Gas Permeability of Fractured Sandstone/Coal Samples under Variable Confining Pressure

Weiqun Liu · Yushou Li · Bo Wang

Received: 26 January 2009 / Accepted: 22 June 2009 / Published online: 8 July 2009

Abstract Rock fractures transmit underground gas effectively once they have sufficient widths and interconnection. However, the fracture geometries needed for gas transport are strongly influenced by surrounding pressure conditions. In order to inspect and quantify the influence of surrounding pressure, we design and manufacture a set of gas flow apparatus that can be connected to the MTS815 material testing system, which provides loads and exhibits external pressures in the experiment. With the apparatus and MTS815, we test the fractured samples of sandstone and coal and obtain their relationship between permeability and external pressure. In particular, our permeability calculation based on collection of gas flux and pressure difference has involved the influence of non-Darcian flow. In addition, our study also includes a numerical simulation in the RFPA software platform to display the internal field changes of cracks. The results show that fracture permeability strongly depends on confining pressure, and a critical pressure probably occurs, about 1.5–2 MPa in our experiments, to split each of the permeability curves into two stages, a slow climb and an exponential rush. As a complement, the numerical simulation also demonstrates one more stage for the permeability curve, the post-rush steady fluctuation.

Keywords Fractured sandstone/coal · Gas permeability · Variable confining pressure · Testing · Numerical simulation

W. Liu
Department of Earth and Planetary Science, University of California, Berkeley, CA 94720, USA
e-mail: wqliu@berkeley.edu

W. Liu (✉) · Y. Li · B. Wang
College of Sciences, China University of Mining and Technology, Xuzhou 221008, China
e-mail: wqliu@cumt.edu.cn

Y. Li
e-mail: li_yushou@163.com

B. Wang
e-mail: aboluocn@126.com

1 Introduction

Fractured rocks are important natural and engineering porous media. However, so far, most research about the flow in rocks only involves undamaged rocks because the flow characteristics in them are more regular and the experiment methods are also relatively simple (Biot 1941; Gong and Xie 1989; Bear and Bachmat 1990; Boer and Ehlers 1990; Smeulders et al. 1992; Springer et al. 1998; Thauvin and Mohanty 1998).

Measuring the flow in fractured rocks can be traced to Lomize's 1951 study in which a parallel-plates model was put forward to simulate the fluid flow in fractures (Witherspoon 1977). After that, researchers also suggested many other approximate models or approaches such as the fracture-geometries measurement, nail-plates similarity, cavity similarity, cavity-lumps model, shear-flow coupling, electrical-resistivity method, transient-pressure testing and steady-flow testing (Snow 1968; Gangi 1978; Walsh 1979; Tsang and Witherspoon 1981; Liu et al. 2003). Recently, Miao et al. (2004) specially built a hollow cylinder apparatus to measure water flow passing through accumulating rock blocks in a deformation-restricted condition, their study involving the non-Darcian flow.

In order to monitor gas flow in fractured porous media, Somerton et al. (1975) have developed an indirect sonic-velocity evaluation technique to measure coal specimen permeability of nitrogen or methane gas, as well as its stress-dependent effects. In addition, Gascoyne and Wuschke (1997) conducted a point-station survey, by collecting gas flow velocity and arrival time at fixed points, to investigate helium gas transport through a water-saturated granitic fracture zone at about 40-m deep underground. Leven et al. (2004) built a single well/hole method, by measuring pneumatic discharge of pressure and flux through a pre-bored well/hole, to provide an insight into processes of air flow occurring in unsaturated fractured sandstone blocks. Of late, Davy et al. (2007) have tried combining external pressure change with fracture permeability measurement. They employed steady-flow and transient-pressure methods for Argon gas and water testings, respectively. However, their permeability was not calculated from gas flow data, but from the difference of specimen diameters for two different external pressures.

Since external confining pressure can dominate fractures' permeability and furthermore gas flow through fractures has a distinct non-Darcian behavior (Miao et al. 2004), in this article, we will introduce the non-Darcian condition in measuring, calculating, and quantifying the influence of external pressure change on fractures gas permeability. The study includes to design and manufacture a set of gas flow apparatus that can be connected to the MTS815 material testing system, to pre-compress (to the peak stress) and seal the samples of sandstone and coal which are usual rock materials in petroleum or mining engineering, to deduce a non-Darcian permeability equation and summarize the relationship between external confining pressure and fracture permeability, and to numerically simulate gas flow in fractures under external pressure change and complement the permeability–confinement-dependent conclusion.

2 Experiment System and Non-Darcian Approach

The MTS loading machine and a self-made gas flow apparatus are two major components in our testing system. Figures 1 and 2, respectively, illustrate the system connection and principle. The gas flow apparatus is composed of a gas cylinder, a relief valve, flux meters, a fractured specimen, pressure difference meters, digital display attachments, high-pressure pipes, gas accumulator, etc. It produces only 5% pressure drop for a 5 MPa gas per 10 min.

Fig. 1 Testing system of gas permeability of rock under confined pressure. *Notes*: (1) Nitrogen cylinder and relief valve; (2) Testing box of gas flow including flow meter, pressure difference meter and accumulator; (3) Load control cabinet; (4) MTS test platform and fractured specimen

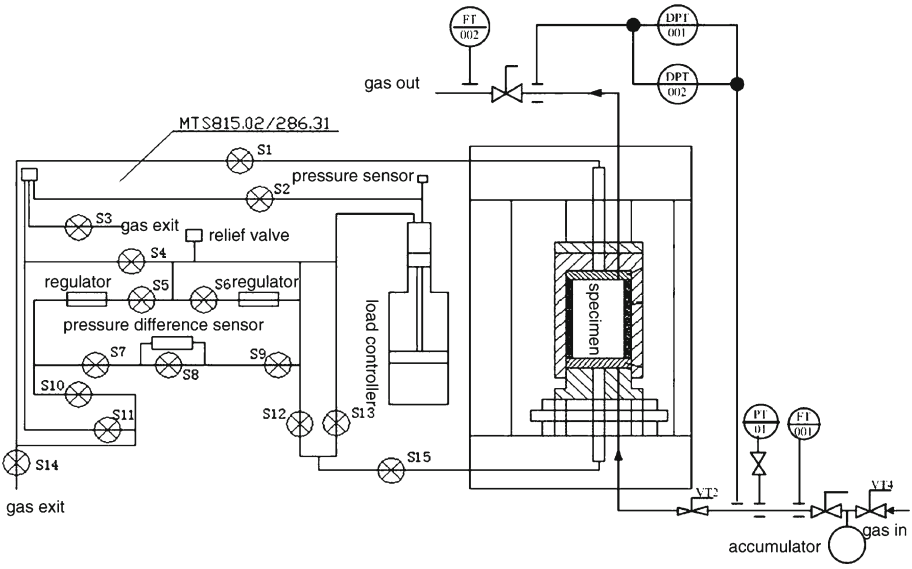

Fig. 2 Testing principle of gas permeability of rock under confined pressure

The MTS815 can independently accomplish water seepage testing under both uniaxial and triaxial conditions; however, without a gas flow auxiliary apparatus, it cannot realize gas seepage testing. The designed and machined unique high-pressure joints for interconnection of gas pipes and MTS water pipes are also key components of the system. Table 1 gives the testing specification of the entire system.

Sample raw materials are sandstone and coal blocks collected from about −300 m strata of Huainan-Guqiao mine. They are machined into cylinders of 50 mm diameter and 100 mm length according to the international standard (ISO22475-1:2006). Before seepage testing,

Table 1 Testing specifications of gas permeability system

Technical item	Specification
Axial load	<1,700 kN
Confining pressure	<45 MPa
Pore water pressure	<45 MPa
Maximum specimen diameter	100 mm
Maximum specimen length	200 mm
Gas flux range	0–5 L/min
Gas pressure difference range	0–6 MPa

Fig. 3 Fractured sandstone specimens after uniaxial compression

these cylinders must undergo uniaxial compression until the stresses start to generate macro cracks—this condition is termed as the peak stress (Figs. 3, 4). The averaged strengths of samples are about 30 MPa for sandstone and 12 MPa for coal. After pre-fractured, the specimens are circumferentially sealed in PVC bands and thermoshrinking plastic covers, fixed onto the MTS testing platform, and then changing side pressures as well as constant axial loads are applied (Fig. 5).

Since cracks have relatively high permeabilities (Leven et al. 2004; Miao et al. 2004), the steady-flow method is selected here, and specimen dimensions, flux, and seepage pressure difference between input and output must be measured for calculating the permeability. The Non-Darcian permeability equation is deduced as follows.

For an one-dimensional non-Darcian flow, the relationship between pressure and flow velocity can be expressed as

$$\frac{\mathrm{d}p}{\mathrm{d}x} = -\left(\frac{\mu}{k}V + \beta\rho V^2\right), \tag{1}$$

where $\mathrm{d}p/\mathrm{d}x$ is the pressure gradient, V is the seepage velocity, μ is the kinetic viscosity, k is the permeability, ρ is the mass density, and β is the non-Darcy factor. If a steady flow dominates testing, Eq. 1 can be simplified to

$$\frac{p_i - p_o}{L} - \beta\rho V^2 = \frac{\mu V}{k}, \tag{2}$$

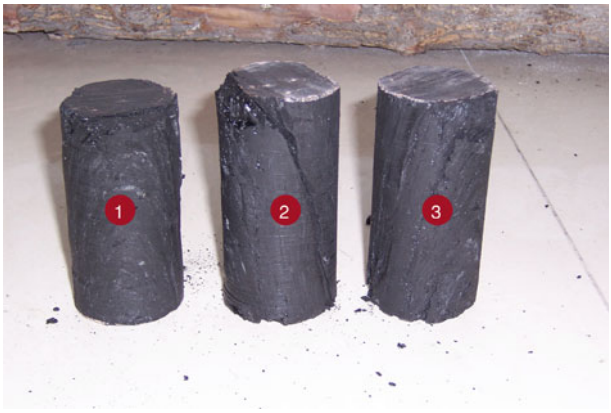

Fig. 4 Fractured coal specimens after uniaxial compression

Fig. 5 A sealed specimen being fixed to the MTS test platform

where p_i is the input pressure, p_o is the output pressure, and L is the specimen length.

By substituting $V = Q/A$ into Eq. 2, where Q is the gas flux and $A = \pi(d^2 - d_0^2)/4$ is the specimen cross-section fractures area (d and d_0 are the respective specimen diameters after and before pre-fracturing), we can calculate the permeability k once pressure difference and flux are measured twice with different values.

$$k = \frac{\mu L}{A} \times \frac{(Q' - Q)QQ'}{(p_i - p_o)Q'^2 - (p_i' - p_o')Q^2}, \tag{3}$$

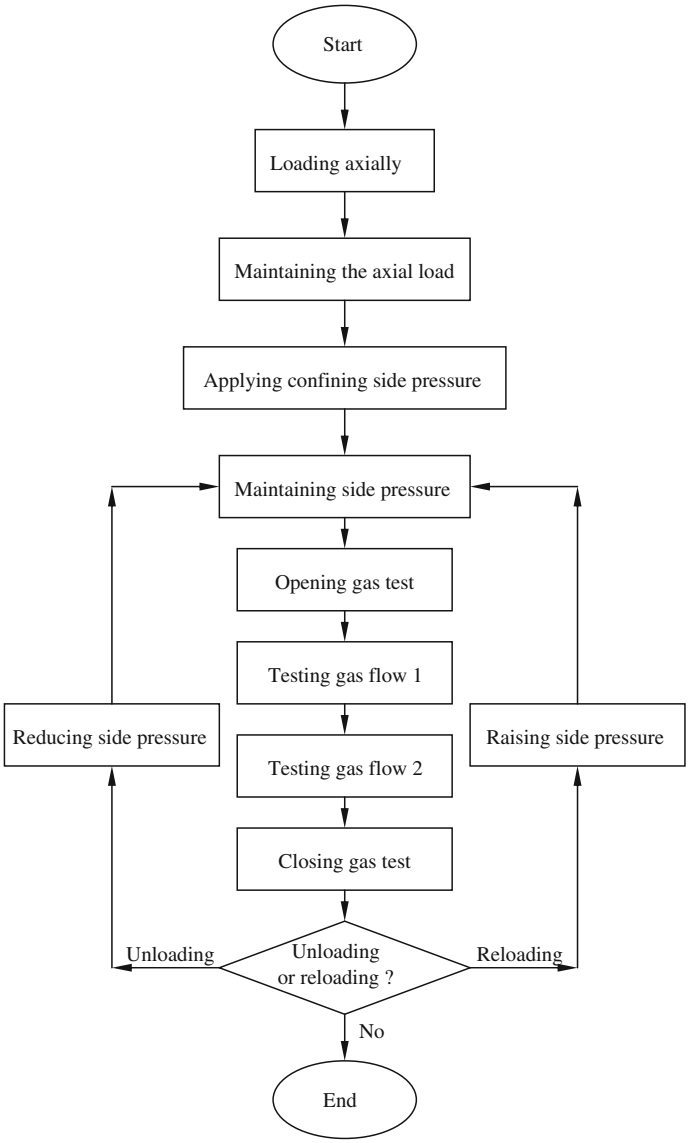

Fig. 6 Testing procedure of gas permeability of rock under changeable confining pressure

where variables with primes correspond to another group of measurements for the same specimen.

The testing gas is nitrogen gas with $\mu = 0.176 \times 10^{-4}$ Pa s and $\rho = 1.16\,\mathrm{kg/m^3}$ at the standard state. In order to obtain stable readings, we arrange gas flow measuring after the axial load and confining pressure are both paused at fixed levels, in other words, load change and gas flow, respectively, belong to two different testing stages. Figure 6 is the entire experiment procedure.

Table 2 Gas permeability test results of the sandstone Sample 1

Confining pressure (MPa)	Input gas pressure (MPa)	Output gas pressure (MPa)	Gas flux ($L\,min^{-1}$)	Permeability ($\times 10^{-14} m^2$)
5.00	0.501/0.501	0.135/0.134	0.495/0.509	1.08
4.00	0.499/0.498	0.137/0.135	0.642/0.657	1.42
3.00	0.502/0.503	0.142/0.143	0.951/0.968	1.99
2.00	0.499/0.501	0.151/0.152	1.422/1.452	3.31
1.00	0.502/0.501	0.184/0.182	2.680/2.690	10.89

Table 3 Gas permeability test results of the sandstone Sample 2

Confining pressure (MPa)	Input gas pressure (MPa)	Output gas pressure (MPa)	Gas flux ($L\,min^{-1}$)	Permeability ($\times 10^{-14}\,m^2$)
5.00	0.414/0.402	0.129/0.028	0.211/0.148	0.28
4.00	0.400/0.399	0.129/0.128	0.149/0.148	0.41
3.00	0.399/0.409	0.129/0.132	0.181/0.230	0.59
2.00	0.403/0.402	0.131/0.131	0.306/0.338	0.87
1.00	0.399/0.400	0.186/0.187	0.631/0.665	2.27

Table 4 Gas permeability test results of the coal Sample 1

Confining pressure (MPa)	Input gas pressure (MPa)	Output gas pressure (MPa)	Gas flux ($L\,min^{-1}$)	Permeability ($\times 10^{-14}\,m^2$)
3.00	0.280/0.281	0.100/0.101	0.124/0.125	0.52
2.50	0.274/0.273	0.101/0.100	0.168/0.169	0.73
2.00	0.280/0.281	0.100/0.101	0.205/0.206	0.85
1.50	0.278/0.279	0.102/0.103	0.178/0.179	0.76
1.00	0.277/0.278	0.102/0.103	0.338/0.339	1.45

3 Testing Results and Permeability–confinement Relationship

In the experiment, the axial load for testing of sandstone permeability is fixed at 5 MPa, and then, the confining side pressure is unloaded from 5 to 1 MPa in four uniform steps. Coal specimens have the fixed axial load of 3 MPa and confining pressure reduced from 3 to 1 MPa in 0.5 MPa increment. Tables 2, 3, 4, and 5 and the upper five rows in Table 6 show testing results and permeabilities calculated from Eq. 3. Figures 7, 8, 9, and 10 and Line 1 in Fig. 11 are permeability–confinement curves.

In Tables 2, 3, 4, 5, and 6, it is found that all specimens gain permeability, as confining pressures are reduced. Moreover, Figures 7, 8, 9, 10, and 11 illustrate that these permeability increases can be divided into two stages, a slow power-functional climb and an exponential rush. Tables and figures also exhibit that the critical confining pressures for climb–rush shifts are located at 1.5–2 MPa or so for almost all our specimens.

Undoubtedly, crack recovery and widening due to surrounding pressure decrease contribute mostly to permeability growth. An exception is the abnormal drop in permeability at a

Table 5 Gas permeability test results of the coal Sample 2

Confining pressure (MPa)	Input gas pressure (MPa)	Output gas pressure (MPa)	Gas flux ($L\,min^{-1}$)	Permeability ($\times 10^{-14}\,m^2$)
3.00	0.164/0.165	0.100/0.101	0.124/0.123	1.44
2.50	0.165/0.166	0.100/0.102	0.168/0.169	1.94
2.00	0.163/0.165	0.101/0.103	0.205/0.206	2.48
1.50	0.134/0.133	0.101/0.100	0.148/0.147	3.34
1.00	0.134/0.135	0.101/0.102	0.328/0.332	7.47

Table 6 Gas permeability test results of the coal Sample 3

Confining pressure (MPa)	Input gas pressure (MPa)	Output gas pressure (MPa)	Gas flux ($L\,min^{-1}$)	Permeability ($\times 10^{-14}\,m^2$)
3.00	0.191/0.190	0.104/0.103	0.088/0.089	0.76
2.50	0.192/0.193	0.104/0.105	0.137/0.138	1.17
2.00	0.184/0.185	0.103/0.104	0.150/0.151	1.39
1.50	0.178/0.180	0.103/0.105	0.185/0.186	1.85
1.00	0.145/0.146	0.100/0.101	0.207/0.208	3.45
1.50	0.183/0.185	0.106/0.108	0.276/0.274	2.70
2.00	0.180/0.182	0.108/0.110	0.195/0.194	2.02
2.50	0.203/0.201	0.106/0.104	0.166/0.164	1.27
3.00	0.385/0.394	0.114/0.113	0.190/0.213	0.65

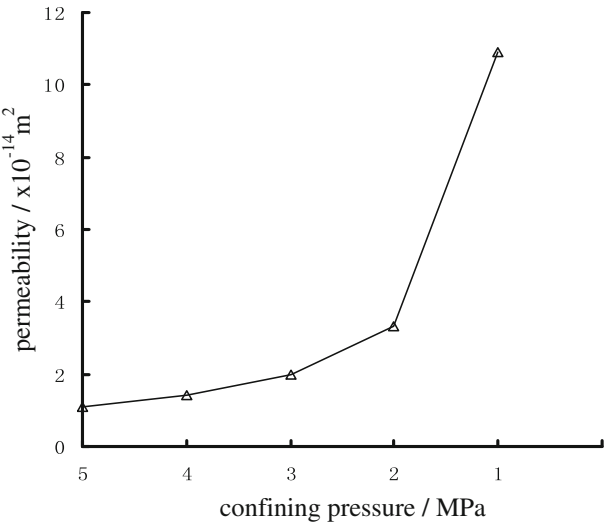

Fig. 7 Gas permeabilities of the sandstone Sample 1 during side unloading

confining pressure of 1.5 MPa in Table 4. This is probably the consequence of gravel particle accumulation in widened fractures and restricting flow. At the critical pressure, isolated cracks are able to complete the transformation from self-expansion to interconnection, and

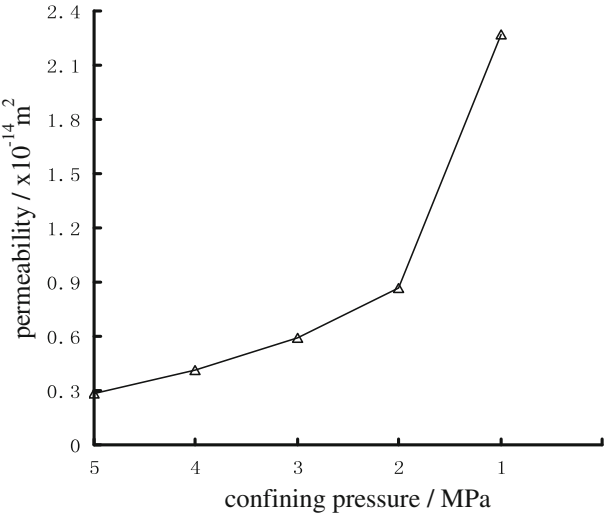

Fig. 8 Gas permeabilities of the sandstone Sample 2 during side unloading

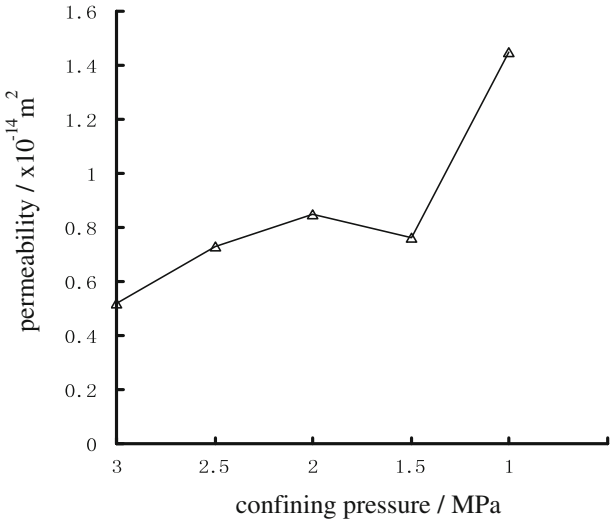

Fig. 9 Gas permeabilities of the coal Sample 1 during side unloading

so permeability rapidly grows. In addition, compared with sandstone, coal seems to have a less distinct critical pressure. A rational explanation is that coal samples suffer more serious damage at the peak-value stress and thereby generate many more cracks that increase permeability before unloading.

Since sandstone and coal are applied with different maximum confining pressures, we further define a relative unloading rate, the ratio of total pressure drop to the maximum pressure, to clearly compare permeability sensitivity to unloading (see Table 7). The results show that at the unloading beginning (unloading rates 17–20%), coal permeabilities have a little more sensitive reaction than sandstone ones, averagely exceeding by about 4%; reversely, at high

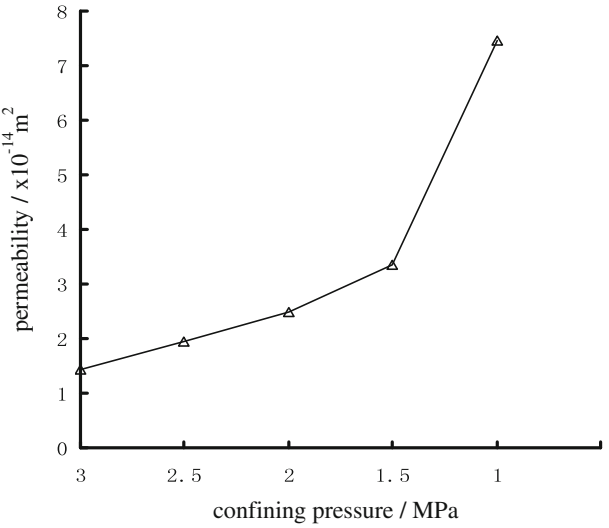

Fig. 10 Gas permeabilities of the coal Sample 2 during side unloading

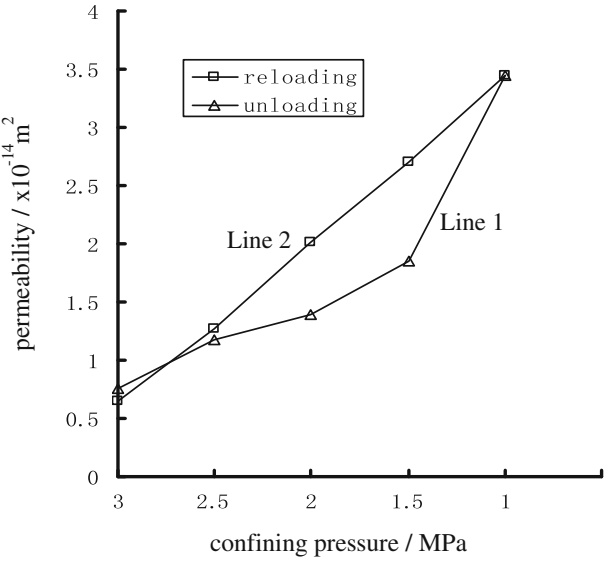

Fig. 11 Gas permeabilities of the coal Sample 3 during side un- and reloading

unloading rates (67–80%), sandstone specimens gain permeability much more rapidly, almost double the biggest increment of coal permeability.

In order to investigate the impact of a load cycle on permeability, we reload 1–3 MPa confining pressure on the coal Sample 3 after unloading of 3–1 MPa. Table 6 and Fig. 11 display the entire permeability changes throughout this load cycle. During unloading, Sample 3 has the same permeability feature as Samples 1 and 2, i.e., two characteristic stages. However, during reloading, permeability declines nearly in a straight line ($R^2 = 0.9991$). This is probably because the loading–unloading–reloading course generates abundant and extensive distributed cracks in the samples, so that cracks can gradually get interconnected

Table 7 Gas permeability growth percentage for different unloading rates

Unloading rate (%)	Sandstone 1 (%)	Sandstone 2 (%)	Coal 1 (%)	Coal 2 (%)	Coal 3 (%)
17	–	–	40.4	34.7	53.9
20	34.0	46.4	–	–	–
33	–	–	63.5	72.2	82.9
40	84.3	110.7	–	–	–
50	–	–	46.2	131.9	143.4
60	206.5	210.7	–	–	–
67	–	–	188.5	418.8	353.9
80	908.3	710.7	–	–	–

Note: the percentage $= (k - k_0)/k_0 \times 100\%$, where k_0 is the permeability at no unloading

and thereby permeability increases more smoothly. It is this uniform permeability growth that contributes to the linear relationship.

4 RFPA Numerical Simulations

In order to support the experimental results and enrich analysis, we employ the numerical software RFPA (see http://www.rfpa.cn/en/e_index.jsp) to simulate fracture gas seepage in the same conditions. RFPA is a FEM-based program in which both, strength/modulus degradation due to solid damage and solid–gas interaction, are simulated. In addition, the Weibull function and Monte-Carlo method are also applied to accomplish heterogeneous distribution of material properties in the model domain. Equations 4–6 are the governing equations for property distributing, material weakening, and state coupling, respectively.

$$f(\theta) = m\frac{\theta^{m-1}}{\theta_0}\exp\left(-\frac{\theta^m}{\theta_0}\right), \tag{4}$$

where θ represents an arbitrary material parameter such as seepage coefficient, θ_0 is its mean, and m is the heterogeneity coefficient. Material properties become more and more heterogeneous as m increases.

$$\begin{cases} \sigma_i = 3\kappa\varepsilon_v + 2G\varepsilon_i(1-D) \\ \lambda = \xi(D)\lambda_0 e^{-\delta(\sigma_1 - \alpha p)} \end{cases}, \tag{5}$$

where κ is the Lamé constant, G is the shearing modulus, ε_v is the volume strain, $D(0 \le D \le 1)$ is the damage factor, $\lambda = k/2\mu P_0$ is the gas seepage coefficient, P_0 is a unit standard atmospheric pressure, λ_0 is the gas seepage coefficient at no material damage, $\xi(D)$ is the magnification coefficient depending on D, δ is the coupling factor, σ_1 is the maximum principal stress, α is the effective stress coefficient, and p is the gas pressure.

$$\begin{cases} (2P_0\lambda_i p_{,i}^2)_{,i} = \dfrac{n}{p}\dfrac{\partial p^2}{\partial t} - 2p\dfrac{\partial \varepsilon_v}{\partial t} \\ (\kappa + G)u_{j,ji} + Gu_{i,jj} + \alpha p_{,i} + F_i = 0 \end{cases}, \tag{6}$$

where n is the porosity, u is the displacement, and F_i is the volume force density.

In order to accord with the experimental specimen, the numerical model's domain is 100 mm long and 25 mm wide in axisymmetry. Figure 12 displays the model outline and

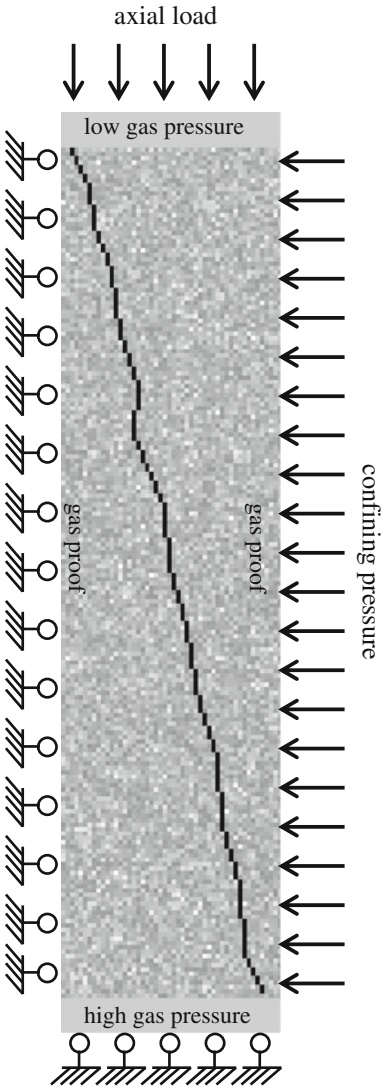

Fig. 12 Numerical model of fracture gas seepage with side unloading

its boundary conditions and Table 8 lists the main calculating parameters. In calculation, the model is meshed into 100 × 25 four-node rectangular elements. The calculated results corresponding to a cracked coal sample is shown in Fig. 13.

As shown in Eq. 5 or 6, the outputs of RFPA do not include permeability k, but gas seepage coefficient λ instead. However, $\lambda = k/2\mu P_0$, and μ and P_0 are constants, and so gas seepage coefficient and permeability have similar pressure-dependent relationships. Therefore, the following discussion does not distinguish between them. Figure 13 illustrates that during unloading from 3 to 1 MPa, permeability/gas seepage coefficient calculated from the model have similar behavior to that produced from the experiment. The simulations also suggest that unloading from 1 MPa or less can lead to a fluctuation of permeability. The fluctuation is a

Table 8 Parameters of numerical simulation of fracture gas seepage with side unloading

Parameter	Value	Parameter	Value
Young's modulus of matrix body	10.0 GPa	Heterogeneity coefficient	1.5
Young's modulus of end parts	200.0 GPa	Coupling coefficient	0.1
Young's modulus of fracture	1.0 kPa	Failure criterion	Mohr–Coulomb
Poisson's ratio	0.3	Friction angle	30°
Gas seepage coefficient of matrix body	0.1 $m^2/(MPa^2$ day)	Axial load	3.0 MPa
Gas seepage coefficient of end parts	100.0 $m^2/(MPa^2$ day)	Side unloading step length	0.1 MPa
Gas seepage coefficient of fracture	500.0 $m^2/(MPa^2$ day)	High gas pressure	1.0 MPa
Uniaxial compression strength of matrix	12.0 MPa	Low gas pressure	0.1 MPa

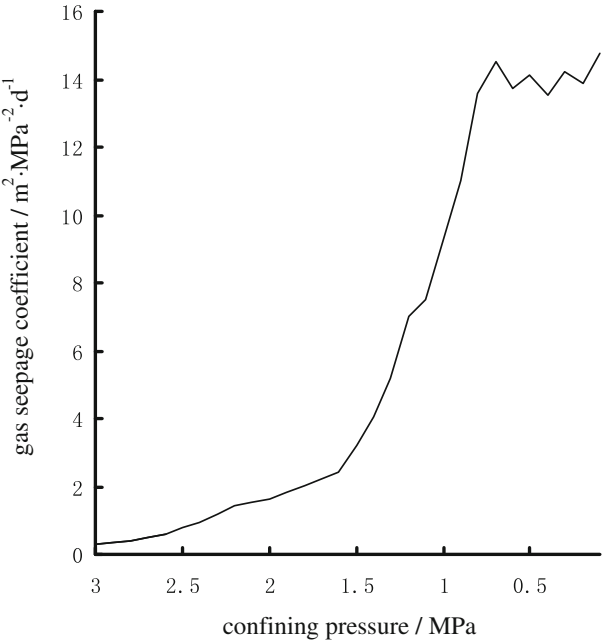

Fig. 13 Numerical results of fracture gas seepage with side unloading

small-scale perturbation of about 5% of the approximately constant value of 14 m^2 MPa d^{-1} seepage coefficient at confining pressures much less than the injecting gas pressure 1 MPa. In order to explain this phenomenon, we try altering the values of injecting gas pressure from 2 to 1 MPa and to 0.5 MPa along with no change of exit pressure of 0.1 MPa and find that the perturbations can always appear, and furthermore start later and later as the gas pressure decreases. As a rational explanation, the appearance of the perturbations is probably based on a kind of inter-feedback: first, high gas pressures may overweigh confining pressures and consequently increase permeability by dilating fractures; inversely, permeability upgrading may accelerate delivering gas to the exit of low pressure and thereby relieve action of high pressure in fractures, leading to shrinking of fractures and decreasing of permeability. No perturbation in the experiments is because the experimental gas pressures are far less than side-confining loads.

5 Conclusions

We studied the impact of variable confining pressure on gas permeability of rock fractures by developing an experiment based on a self-designed gas flow apparatus, the MTS system, and a non-Darcian testing method. Simulations of these experiments were carried out by employing the RFPA numerical software. The main conclusions are as follows.

(1) As confining pressure is gradually reduced, the gas permeability of rock fractures increases, and the increase can be divided into two stages—slow power-functional increase and exponential rush. In our experiment, 1.5–2 MPa is a critical pressure for the division of these stages, and furthermore, the critical pressure for sandstone is more distinct than that for coal.
(2) Compared with those of sandstone, fractured samples of coal react and increase permeability more quickly at the beginning of unloading. However, after full unloading, the total permeability increment of a sandstone sample is more than that of a coal sample. If a fractured specimen undergoes reloading after unloading, with the load increased, the permeability almost linearly decreases.
(3) Numerical simulation also indicates that permeability increase includes first slow climb and then sudden rush. Moreover, the simulation suggests a small-scale steady fluctuation appearing after the rush stage, and the fluctuation range is about 5% of the seepage coefficient.

Acknowledgements The authors highly appreciate the reviewers' suggestions. This study was supported by National Natural Science Foundation of China (No. 50774083), Chinese Program for New Century Excellent Talents in University (No. NCET-07-0803) and Special Subject Grant of National "973" Basic Research Program of China (No. 2005CB221502).

References

Bear, J., Bachmat, Y.: Introduction to Modeling of Transport Phenomena in Porous Media. Kluwer, Norwell MA (1990)

Biot, M.A.: General theory of three-dimensional consolidation. Int. J. Appl. Phys. **12**, 155–164 (1941). doi:10.1063/1.1712886

Boer, R.D., Ehlers, W.: Development of the concept of effective stresses. Acta Mech. **83**, 77–92 (1990). doi:10.1007/BF01174734

Davy, C.A., Skoczylas, F., Barnichon, J.D. et al.: Permeability of macro-cracked argillite under confinement: gas and water testing. Phys. Chem. Earth Parts A/B/C **32**, 667–680 (2007). doi:10.1016/j.pce.2006.02.055

Gangi, A.F.: Variation of whole and fractured porous rock permeability with confining pressure. Int. J. Rock Mech. Min. Sci. Geomech. Abstr. **15**, 249–257 (1978). doi:10.1016/0148-9062(78)90957-9

Gascoyne, M., Wuschke, D.M.: Gas migration through water-saturated, fractured rock: results of a gas injection test. J. Hydrol. (Amst.) **196**, 76–98 (1997). doi:10.1016/S0022-1694(96)03305-7

Gong, Y.G., Xie, Y.D.: A review of laboratory investigation of rock permeability. Chin. J. Rock. Mech. Eng. **8**, 219–227 (1989)

Leven, C., Sauter, M., Teutsch, G. et al.: Investigation of the effects of fractured porous media on hydraulic tests—an experimental study at laboratory scale using single well methods. J. Hydrol. (Amst.) **297**, 95–108 (2004). doi:10.1016/j.jhydrol.2004.04.004

Liu, W.Q., Miao, X.X., Chen, Z.Q.: A testing method for determining the permeability of overbroken rock. Chin. J. Exp. Mech. **18**, 56–61 (2003). doi:10.3901/JME.2003.07.056

Miao, X.X., Liu, W.Q., Chen, Z.Q.: Seepage Theory of Mining Strata. Science Press, Beijing (2004)

Smeulders, D.M.J., Eggls, R.L.G.M., Dongen, M.E.H.V.: Dynamic permeability: re formulation of theory and new experimental and numerical data. J. Fluid Mech. **245**, 211–227 (1992). doi:10.1017/S0022112092000429

Snow, D.T.: Rock fracture spacings, openings and porosities. J. Soil Mech. Found Div., Proc. ASCE **94**, 73–91 (1968)

Somerton, W.H., Söylemezolu, I.M., Dudle, R.C.: Effect of stress on permeability of coal. Int. J. Rock Mech. Min. Sci. Geomech. Abstr. **12**, 129–145 (1975). doi:10.1016/0148-9062(75)91244-9

Springer, D.S., Loaiciga, H.A., Cullen, S.J. et al.: Air permeability of porous materials under controlled laboratory conditions. Ground Water **36**, 558–565 (1998). doi:10.1111/j.1745-6584.1998.tb02829.x

Thauvin, F., Mohanty, K.K.: Network modeling of non-Darcy flow through porous media. Transp. Porous Media **31**, 19–37 (1998). doi:10.1023/A:1006558926606

Tsang, Y.W., Witherspoon, P.A.: Hydromechanical behavior of a deformable rock fracture subject to normal stress. J. Geophys. Res. **86**, 9187–9198 (1981). doi:10.1029/JB086iB10p09287

Walsh, J.B.: A new model for analyzing the effect of fracture on compressibility. J. Geophys. Res. **84**, 3532–3536 (1979). doi:10.1029/JB084iB07p03532

Witherspoon, P.A.: Mechanical and hydraulic properties of rock related to induced seismicity. Eng. Geol. **11**, 35–45 (1977)